AD-A194 705 EXPERIMENTAL DETERMINATION OF DRAG MODIFICATIONS DUE TO ELASTIC COMPLIANT.. (U) MICHIGAN STATE UNIV EAST LANSING TURBULENCE STRUCTURE LAB R E FALCO ET AL. 27 APR 88 1/1

UNCLASSIFIED TSL-88-2 N00014-82-K-0348 F/G 20/4 NL

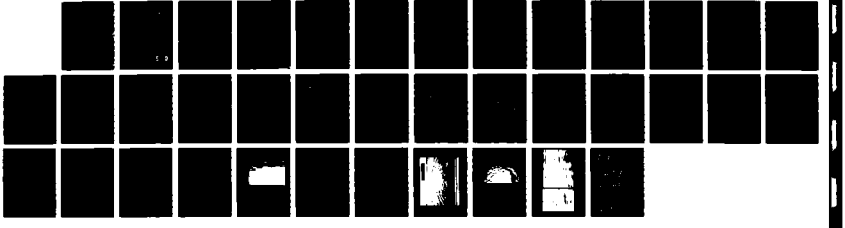

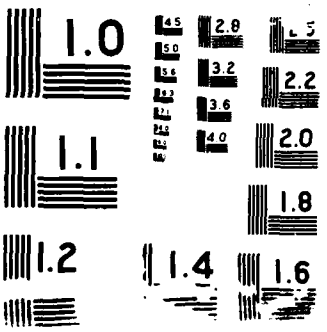
1.0
1.1
1.2
1.4
1.6
1.8
2.0
2.2
2.8
3.2
3.6
4.0

EXPERIMENTAL DETERMINATION OF DRAG MODIFICATIONS DUE TO ELASTIC COMPLIANT SURFACES USING QUANTITATIVE VISUAL TECHNIQUES

by

R. E. Falco and C. C. Chu

Final Technical Report

Prepared from work done under
Office of Naval Research
Contract N00014-82-K-0348

Report TSL 88-2

Turbulence Structure Laboratory
Department of Mechanical Engineering
Michigan State University
East Lansing, MI 48824

April 1988

REPORT DOCUMENTATION PAGE

1a. REPORT SECURITY CLASSIFICATION Unclassified	1b. RESTRICTIVE MARKINGS
2a. SECURITY CLASSIFICATION AUTHORITY	3. DISTRIBUTION / AVAILABILITY OF REPORT Unlimited
2b. DECLASSIFICATION / DOWNGRADING SCHEDULE	
4. PERFORMING ORGANIZATION REPORT NUMBER(S)	5. MONITORING ORGANIZATION REPORT NUMBER(S)
6a. NAME OF PERFORMING ORGANIZATION Michigan State University 6b. OFFICE SYMBOL (If applicable)	7a. NAME OF MONITORING ORGANIZATION Office of Naval Research
6c. ADDRESS (City, State, and ZIP Code) East Lansing, MI 48824	7b. ADDRESS (City, State, and ZIP Code) Office of Naval Research Code 438 Arlington, VA
8a. NAME OF FUNDING / SPONSORING ORGANIZATION ONR 8b. OFFICE SYMBOL (If applicable)	9. PROCUREMENT INSTRUMENT IDENTIFICATION NUMBER Contract N00014-82-K-0348
8c. ADDRESS (City, State, and ZIP Code) Office of Naval Research Code 438 Arlington, VA	10. SOURCE OF FUNDING NUMBERS PROGRAM ELEMENT NO. / PROJECT NO. / TASK NO. / WORK UNIT ACCESSION NO.

11. TITLE (Include Security Classification)
Experimental Determination of Drag Modifications Due to Elastic Compliant Surfaces Using Quantitative Visual Techniques

12. PERSONAL AUTHOR(S)
R. E. Falco & C. C. Chu

13a. TYPE OF REPORT	13b. TIME COVERED	14. DATE OF REPORT (Year, Month, Day)	15. PAGE COUNT
Final	FROM 1982 TO 1985	88-4-27	35

16. SUPPLEMENTARY NOTATION

17. COSATI CODES			18. SUBJECT TERMS (Continue on reverse if necessary and identify by block number)
FIELD	GROUP	SUB-GROUP	Compliant Surfaces, Skin Friction, Drag Reduction, Boundary Layers

19. ABSTRACT (Continue on reverse if necessary and identify by block number)

Direct measurements of the wall shear stress have been made at a point on three thicknesses of an elastic compliant surface. Approximately 8% C_f reduction was measured on each surface. Observations of the surfaces' motion showed that they responded to the microscale turbulent eddies. At higher forcing the onset of various surface wave phenomena were observed.

20. DISTRIBUTION / AVAILABILITY OF ABSTRACT ☒ UNCLASSIFIED/UNLIMITED ☐ SAME AS RPT. ☐ DTIC USERS	21. ABSTRACT SECURITY CLASSIFICATION Unclassified
22a. NAME OF RESPONSIBLE INDIVIDUAL	22b. TELEPHONE (Include Area Code) / 22c. OFFICE SYMBOL

1. INTRODUCTION

Over the past few years there has been a renewed interest in the possibility of lowering skin friction drag caused by turbulent boundary layers through the use of compliant surfaces. These are surfaces that will deform under the shear stress and pressure fluctuations created by turbulence. This deformation can result in significant changes in flow properties. It has been suggested that this ability to deform the surface may inhibit the process by which turbulence is produced, thus lowering the drag. The detailed mechanism by which this will occur is not yet completely understood. To determine whether or not a compliant surface reduces the skin friction drag, only three types of measurement are possible: momentum balances, drag balances and obtaining $\partial u/\partial y$ at the wall with a non-disturbing measurement technique. Drag balance measurements have been made by several investigators for PVC based visco-elastic surfaces such as Hansen et al. (1974). On the whole, these show an increase in drag that has been attributed to the formation of static divergence waves in the surface. Recently, elastic surfaces have been investigated (Gad-el-Hak 1984). These experiments showed the formation of smaller and faster waves. However, no drag measurements have yet been attempted. In principle, no matter how accurate the drag balance measurement is, it cannot give instantaneous shear stress information, which will be needed to determine what aspects of the turbulence production process are interfered with by various wall mechanisms. Although the surface hot-film technique and hydrogen bubble technique are available to get the instantaneous information, yet, the problems of surface interference, buoyancy problems, and flow disturbance problems are still not solved, which make the results questionable. Thus, a non-intrusive wall shear stress measurement technique is needed, which can give accurate results. The photochromic technique can do this. We present the results of skin

friction measurements made on an almost elastic (very low damping) compliant surface. The measurements were made possible by using the single tracer technique. It enabled us to visualize the instantaneous velocity profile in the viscous sublayer region and thus to measure the velocity gradient at the wall directly even though the surface is moving (see the discussion in the chapter about the error analysis).

2. EXPERIMENTAL DETAILS

Experiments were performed in a recirculating channel flow facility, which included 1) overall deformations of the compliant surfaces under turbulent channel flows at fluid to surface wave speed ratios, K, from 0 to 2.2; and 2) measurements of the local skin friction on both stiff surface and compliant surfaces under the identical flow conditions.

2.1. Kerosene channel flow facility

A turbulent channel flow was developed in the 5.49 m by 0.4572 m by 0.1524 m test section of a recirculating liquid flow facility, in which deodorized kerosene was used as the working fluid. The rectangular channel was designed with a 0.4 degree decline angle along the flow direction to remove any air bubble in the channel. The flow was driven by a 2 HP DC motor with a solid state power supply turning an axial pump. The flow was tripped by two 6.35 mm diameter threaded rods which were mounted at the top and the bottom plate of the channel separately. The trip rods were located 6.35 cm downstream of a 20 mesh screen which was at the downstream end of a precise hex honeycomb. The test section hatch (50.8 cm by 25.4 cm) was fitted at the bottom plate and was 4.19 m downstream of the trips. Two viewing windows (45.72 cm by 15.24 cm) were mounted on the side walls of the channel at the test section. A 19 mm quartz laser

access window was mounted flush with the top wall of the channel, allowing measurements to be made 38 cm downstream of the leading edge of the test hatch. Fig. 1 shows a scheme of the experimental apparatus.

The use of approximately 500 gallons of kerosene necessitated some safety precautions. Ten parts per million of the antistatic agent, Shell 71 solution, were added to prevent dangerous electrical charge buildup since the channel was typically run for several hours such that the kerosene reached equilibrium state with ambient temperature before measurements were made. The channel, storage tank and all associated equipment were grounded, and all pump motors were shielded. To achieve high quality of hot-film measurement; a filter made by Flow Tech Co. was also used to eliminate any particles in the kerosene bigger than 0.5 microns.

2.2. Flow documentation in kerosene channel

Velocity profiles were taken using a TSI cylindrical hot-film probe, 1210-20W, and a DISA anemometer, 55M01. The probe was bent into a five degree of pitch angle in order to get several measurements in the near wall region. The probe was calibrated at the center line of the kerosene channel flow by the photochromic single tracer technique. We averaged about 100 velocity values from photos which were taken by a Nikon camera with a micro lens and a motor drive during the probe sampling period. In all, there were ten velocity points calibrated between 0.015 m/sec. and 0.366 m/sec. The laser pulsing rate for each velocity calibration was set from 2 Hz to 25 Hz.

The two-dimensionality of the channel flow was checked from the static pressure drop measurements made at the quarter, half and three-quarter spanwise points every foot along its length. An open type kerosene manometer was used for those measurements. The details of the pressure measurement is also shown in Fig. 1.

2.3. Compliant surfaces

The compliant surfaces were made of Knox unflavored gelatin, which has been found to exhibit nearly elastic properties (see Hunston, Yu and Bullman 1984). Shear moduli G of compliant surfaces were obtained through the relationship $\tau = G \times \gamma$ where τ was the applied shear stress and γ was the shear strain carefully measured by a telescope. Fig. 2 shows the dependence of the shear modulus of gelatin on the concentration of gelatin and water mixture. The concentration is counted as the percentage of the weight of the powder gelatin in the water mixture. The gelatin was put in a refrigerator at 40 degrees F for six hours after it was prepared in the special tray; then we measured the shear modulus of the gelatin prior to testing it in the kerosene channel. The special trays could be inserted into the test section hatch, allowing various thicknesses to be tested. 3 mm, 19 mm and 30 mm thick surfaces were studied, which corresponded from 6 to 60 times the viscous sublayer thickness at $Re_\theta \cong 1200$. The trays were 48 cm long in the streamwise direction and 22 cm wide in the spanwise direction.

2.4. Surface responses on compliant coatings

Preliminary experiments were conducted to study overall surface motion characteristics of compliant surfaces under the turbulent channel flows at different Reynolds numbers. Taking advantage of the total internal reflection at the interface between compliant surface and kerosene (because the index of refraction of the kerosene is greater than that of the gelatin), we were able to study the spatial pattern of the surface motions by visualizing the light which shone through the rear viewing window and was totally reflected at the interface. We set up a 16 mm REDLAKE high speed movie camera looking through one of the viewing windows with a 25 degree pitch angle with respect to the tested surface to capture the surface deformation under the

turbulent channel flow. The sketch of the experimental apparatus is shown in Fig. 3. The surface deformation was recorded on EASTMAN KODAK EKTACHROME 7250 film. The framing rate varied from 100 to 400 frames/second, depending on the channel flow speed. The recorded movie was projected on a 90 by 90 cm diffused glass through a 16 mm PHOTO OPTICAL DATA ANALYZER which has the function of single frame advancing. By the superimposed calibration scale we could obtain length scales, time scales, frequencies of occurrence, and velocity scales associated with various deformation patterns.

2.5. Direct shear stress measurement on the walls

2.5.1. Measurement technique and set-up

The photochromic single tracer technique was used to measure the wall shear stress on both stiff and compliant surfaces. The laser pulses passed through the laser access window and intersected the bottom plate on the tested surfaces. Fig. 4 shows the optical set-up of this experiment. The laser beam was thinned by a 500 mm focal length convex lens to 150 μm at the tested wall. The photochromic time lines were viewed through a short range Questar telescope which enabled us to resolve the motions in the viscous sublayer and its adjacent region, typically, the field of view was 5 mm by 3 mm. The data was recorded by a 35 mm Photosonic high speed movie camera on Kodak TRI-X 400 film. We photographed at a framing rate that allowed two fresh photochromic time lines to be recorded on each frame. The rate of the laser pulse was high enough to have a negligible motion of the compliant surface between two pulses.

The aluminum and gelatin surfaces were reflective enough to result in a sharp reflection of the photochromic time line. The point at which the actual photochromic time line and its image met uniquely defined the instantaneous position of the surface. This fact was used both to define the distance above the surface, and to quantify the

instantaneous motion of the surface. We measured the velocity at a constant distance ($y^+ \cong 4$, where the u_τ was obtained from the Hot film measurement for stiff surface) from the surface, whether it was fixed or moving, by simply measuring the distance between two lines at our chosen distance above the current position of the wall and dividing it by the time between two pulses. Thus, the $\partial u/\partial y$ or wall shear stress value could be obtained from each frame. Fig. 5 shows a close-up of this technique used for wall shear stress measurements on compliant surfaces. In those experiments, a laser pulse rate of 75 Hz and camera framing rate of 25 frames/second were used. All films were analyzed on a NAC motion film analyzer which is accurate to 0.05 mm.

3. Results

3.1. Flow documentation in kerosene channel

3.1.1. Velocity profiles

The standard deviation of the calibration of the hot-film probe was 0.003 m/sec. Fig. 6 shows the mean velocity profile over a stiff surface at the same streamwise location used for the photochromic measurements taken under conditions which lead to skin friction reduction on the compliant surfaces. The centerline velocity was 0.341 m/sec yielding $Re_\theta \cong 1200$. The plot follows the Coles (1968) law of the wall. Fig. 7 shows the turbulent intensity profiles which match those of Eckelmann (1974).

3.1.2. Pressure measurement

The result of the pressure measurement at $Re_\theta \cong 1200$ is shown in Fig. 8, which indicated that there was an even pressure distribution in the spanwise direction of the channel flow and there was a smooth pressure gradient along the channel flow direction.

3.2. Surface responses of compliant coatings in turbulent channel flow

Preliminary experiments were performed to classify the surface responses of the gelatin at different values of flow speed/surface wave speed, K, for three coating thicknesses. Fig. 9 shows the stability boundary for the onset of class B waves for both gelatin and PVC plastisols obtained by Gad-el-Hak et al (1984). It indicates that the onset value of K of wave-like motion for both materials strongly depends on the coating thickness. The current visual observations of 3, 19 and 30 mm thick coatings showed that the first response of all three coatings was with local, three-dimensional, small scale, randomly oriented, and short lived deformations at approximately the same value of K, 0.6, instead of being a wave-like response. This onset response is different from that of the wave-like motion and hasn't been observed by other investigators. The insensitivity of coating thickness to this onset response supported these observation.

As we increased the values of K, we observed the change of the characteristics of the surface responses. The three-dimensional, micro-scaled, and short-lived pocket-like depression (Falco 1980 b), the intermittency of triangular-shaped waves, and the large-scaled quasi two-dimensional waves are the basic elements which constituted the surface responses of the compliant surfaces. The occurrence of each element strongly depended upon the values of K and on the coating thickness. Fig. 10 shows the dependence of the occurrence of each element on both K and coating thickness.

Gad-el-Hak et. al. (1984) showed that wave-like motion on the compliant coatings did increase the drag. It appears that the beneficial range of surface motions might occur between our current onset condition and the onset of the wave-like motions (class B waves).

3.3. Shear stress measurements at walls - both stiff and compliant surface

3.3.1. Results from photochromic technique

We performed experiments to measure the wall shear stress in the possibly beneficial range suggested from the visual results in sec. 3.3.2. The wall shear stresses were obtained using the photochromic single tracer technique at 4.31 m downstream of the trip rod, with centerline velocity 0.341 m/sec yielding $Re_\theta \cong 1200$. The measurement conditions associated with each different thickness are also shown in Fig. 9. Table 1 lists the statistical results of the local skin friction coefficient on both stiff and compliant surfaces.

TABLE 1

Local skin friction coefficient C_f

surface	K	mean	s.d.	skewness	flatness
STIFF		0.004324	0.001277	0.670	3.629
COMPLIANT	overall	0.003966	0.001295	0.685	3.413
3 mm	1.58	0.003950	0.001310	0.760	3.687
19 mm	1.37	0.003976	0.001255	0.500	2.880
30 mm	1.33	0.003973	0.001333	0.810	3.661

Figure 11 shows the histogram of the skin friction obtained from 1205 samples over the reference stiff surface. The curve is a lognormal distribution, which has the same mean and standard deviation as the experimental result shown in 1. Fig. 12 (a) through (c) are the histograms of the skin friction associated with 3, 19 and 30 mm compliant coatings. The curves are also lognormal distributions. If we combine Fig. 12 (a) through (c) regardless of thickness, then we will have the histogram shown in Fig. 13. Comparing the stiff surface (Fig. 11) versus the compliant surfaces (Fig. 13), we have an 8% reduction in skin friction coefficient.

3.3.2. Skin friction measurement on stiff surface by hot-film anemometer

Table 2 shows the results of local skin friction, C_f, obtained from the hot-film measurement under the same flow conditions which led to skin friction reduction on compliant surfaces. The results obtained from the photochromic technique are also shown in Table 2 as reference.

TABLE 2

C_f measurement from Hot-film

# of measurement	C_f (Clauser)	C_f (Newton)
1	0.00460	0.00379
2	0.00455	0.00388
3	0.00455	0.00376
average	0.00457	0.00381
Photochromic technique	0.00432	

3.4. Surface response on compliant surfaces associated with the wall shear stress measurement

Visual observation showed that three-dimensional, short-lived pocket-like depressions, which are of the order of Taylor microscale, formed on the compliant surfaces (see Fig. 14 photo) at the same flow condition at which we conducted the wall shear stress measurement. Those depressions were the major observed response which showed up randomly on the compliant surfaces and were bordered by crests that extended above the mean level of the undisturbed surfaces. Table 3 lists the physical scales associated with the pocket-like depressions. Those data were obtained from the 16 mm movie mentioned in sec. 3.2.4.

Fig. 15 shows the comparison of transverse length scale of depressions in

compliant surfaces with the pocket footprints made on a solid surface. (cf. Yoda, Falco, and Emmerling). The comparison of the time between depressions in compliant surfaces with the time between pocket-like foot prints obtained from boundary layer and channel flows is shown in Fig. 16 (Lovett, Eckelmann, and Thomas).

TABLE 3

Physical scales associated with the pocket-like depressions

thickness	3 mm	19 mm	30 mm	average
K	1.55	1.25	1.25	
log w+	1.92 0.04	1.92 0.04	1.96 0.04	1.93 0.04
T_d+	30.2 1.8	27.8 1.8	33.2 3.8	30.4 2.5
T_b+	35.8 5.4	33.4 4.6	30.9 5.4	33.4 5.1
U_c/U_{cl}	0.59 0.07	0.62 0.07	0.59 0.05	0.60 0.05
max. d	1.2 y+	1.6 y+	1.6 y+	1.5 y+
K used in C_f measurement	1.58	1.37	1.33	

3.5. Observed wave patterns on compliant surfaces

When the value of K was over 1.2 (for thinner coating), groups of three-dimensional triangular-shaped waves were observed intermittently. Fig. 17 is a photo showing this kind of wave. This phenomenon strongly depends on the thickness of the compliant coatings. It appeared at relatively lower values of K for thicker coatings. For 3 mm coating it existed at K between 1.2 and 2.1. As K was below 1.8, the pocket-like depressions dominated the overall picture. However, those triangular-shaped waves were dominant when K was over 1.8. Table 4 shows the wavelength, half angle, wave speed, and wave numbers associated with the triangular-shaped waves in 3 mm coating at two different value of K.

As the value of K was increased, the wave patterns became quasi-two-dimensional and approached two-dimensionality for thicker coatings. Those waves were the large-scale waves with large amplitudes traveling at about 50% of the channel center-line velocity, they looked like the class B waves which were observed by Gad-el-Hak et al. Fig. 18 shows a photo of these quasi two-dimensional large-scaled waves.

TABLE 4

Characteristics of the triangular-shaped waves

flow speed/surface wave speed, K	1.80		2.07	
wavelength/coating thickness	2.89	0.35	3.50	0.31
half angle (degree)	46.7	3.0	52.1	3.3
wave velocity/flow velocity	0.73	0.02	0.72	0.03
wave numbers	2.43	0.56	3.34	0.80

4. Discussion

The lateral scale of the pocket-like depressions is about 60 times the height of the surface movement, so that if a probe was positioned in the wall, it would severely inhibit these motions of the compliant surface. The photochromic technique is a reliable tool to obtain the wall shear stress on compliant surfaces nonintrusively and accurately.

The average reading uncertainty obtained from different readers during the data reduction process through a motion film analyzer was 3%, which was mainly a result of human error. Through the use of digital image processing equipment, this uncertainty can be reduced. The maximum error associated with the $\partial u/\partial y$ measurement caused by the movement of compliant surface was 4%. This error was estimated by the maximum vertical displacement on compliant surfaces between two photochromic time lines. It is

reasonable to use the lognormal distribution to estimate the mean of the error which is due to the surface movement because the wall shear stress has a lognormal distribution. Thus, the mean of the error in calculating $\partial u/\partial y$ is about 1.5%.

Results of hot-film measurement were different from those obtained using the photochromic technique. The result obtained using Clauser plot based on Coles (1968) universal law is about 5% higher than that obtained using the photochromic technique. The reason for this difference may possibly be attributed to measurement error or the favorable pressure gradient of the channel flow which was not fully developed.

The value of $\text{rms}(\partial u/\partial y)/\text{mean}(\partial u/\partial y)$ was 0.295 on the stiff surface measurement; this indicates that the measurement was in agreement with several investigators such as Mitchell & Hanratty (1966) and Eckelmann(1974).

In comparing the two histograms in Fig. 11 and Fig. 13, the compliant surfaces did change the characteristics of the statistical results on skin friction distribution. Interestingly, it shows that only the high probability events have been changed and the skewness and flatness almost stay the same.

The only other study of elastic surfaces known to the author is that of Gad-el-Hak et al.(1984). He found that two-dimensional waves set in at values of K (approximately 3.5, for a 3 mm thick surface) higher than those for which we found a three-dimensional pattern. The reason for the differences are not known, but earlier, Falco, Chu and Wiggert (1983) also observed a three-dimensional pattern developed in the same compliant material in a water channel test before the onset of large amplitude waves of the type found by Gad-el-Hak et al.

It appears that the response we have found is a response of the surface to the microscale eddies of the turbulence, which, at least in these preliminary experiments,

does lead to skin friction reduction. More evidence on this is shown in Table 3; the length scales, the velocity scales and the time scales associated with the pocket-like depressions correlate very well with those of the bursting process in a turbulent channel flow and boundary layer flow. Fig. 15 and Fig. 16 show a very good agreement among the comparisons. Fig. 19 shows the further comparison between the visual phenomena on compliant surfaces and the flow visualization in the near wall region of channel flow by Yoda (1981). Apparently, they look similar.

Interestingly, we obtained almost the same amount of skin friction reduction for three different thickness coatings at the operating conditions. It may suggest that the characteristics of turbulence being modified during the interaction with the compliant surfaces has weak dependence on the thickness of the coating, when the operating value of K is slightly above our current onset boundary and is significantly below the onset boundary of class B waves. If this modification were created by wave motions on compliant surfaces, then the dependence on the coating thickness should be pronounced.

From Fig. 9 we also can see that for thinner coatings there is a wider range of three-dimensional surface deformation before the onset of quasi-two-dimensional surface motions. Thus, thinner coatings should have a wider operating range over which skin friction reductions are possible. Further experiments are needed to determine the range of applicability of these results.

As far as the triangular-shaped waves are concerned, their half angles, wavelengths and wave numbers increased as the value of K went up. Eventually, the half angles reached to 90 degrees and the waves became two-dimensional, which had large amplitude and wavelength spreading over the whole compliant surface. Those large scale waves were close to class B waves observed by Gad-el-Hak et al., which

travelled at about 50% of the channel center line velocity.

5. Conclusions

1. A non-intrusive quantitative photochromic single tracer technique has been used to measure the skin friction both on a stiff surface and on compliant surfaces. The error of this technique is about 4.5% plus sampling error.

2. Eight percent (8%) skin friction reduction has been found on low damping elastic gelatin.

3. Histograms of skin friction distribution are lognormal for both stiff and compliant surfaces.

4. The observed onset response on currently used compliant surfaces was local, three-dimensional, small scale, and short lived deformation at approximately the same value of K, 0.6, for three different thicknesses.

5. In conditions which lead to skin friction reduction, the surface responses show the characteristics of turbulence. The measured length scale, time scales and velocity scale associated with the observed pocket-like depressions correlate very well with those of the bursting process in wall bounded turbulent flows.

REFERENCES

Ecklemann, H. 1974. "The Structure of the Viscous Sublayer and the Adjacent Wall Region in a Turbulent Channel Flow", J.Fluid Mech. 65, p.439.

Emmerling, R. 1973. "The Instantaneous Structure of the Wall Pressure under a Turbulent Boundary Layer Flow", Max-Planck-Institut fur Stromungsforschung Bericht Nr. 9.

Falco, R.E. 1980b. "Structural Aspects of Turbulence in Boundary Layer Flows", in

"Turbulence in Liquids" ed. Patterson and Zakin, pp. 1-15.

Falco, R.E., Chu , C.C., and Wiggert,D.C., 1983. "Experiments on Compliant Surfaces Using Quantitative Visual Technique," Symposium on Drag Reduction, National Science Academy, Washington D.C.

Gal-el-Hak, M, Blackwelder, R.F., and Riley, J.J. 1984. "On the Interaction of Compliant Coatings with Turbulent Boundary Layer Flows", J. Fluid Mech. 140, p.257

Hansen, R.J., Hunston, D.L., Ni, C.C., Reischman, M.M. 1980. "An Experimental Study of Flow-Generated Waves on a Flexible Surface", J. Sound and Vibration 68(3), P.317-334

Hunston, D.L., Yu, C., and Bullman, G.W., 1984. "Mechanical Properties of Compliant Coating Materials", presentes at ASME Energy Sources Technology Conference, Feb. 12-16

Yoda, H. 1981. "Effects of Dilute Polymer Additives on the Turbulence Structure Near a Wall", MS Thesis, Dept. of Mech. Engr., Michigan State Univ.

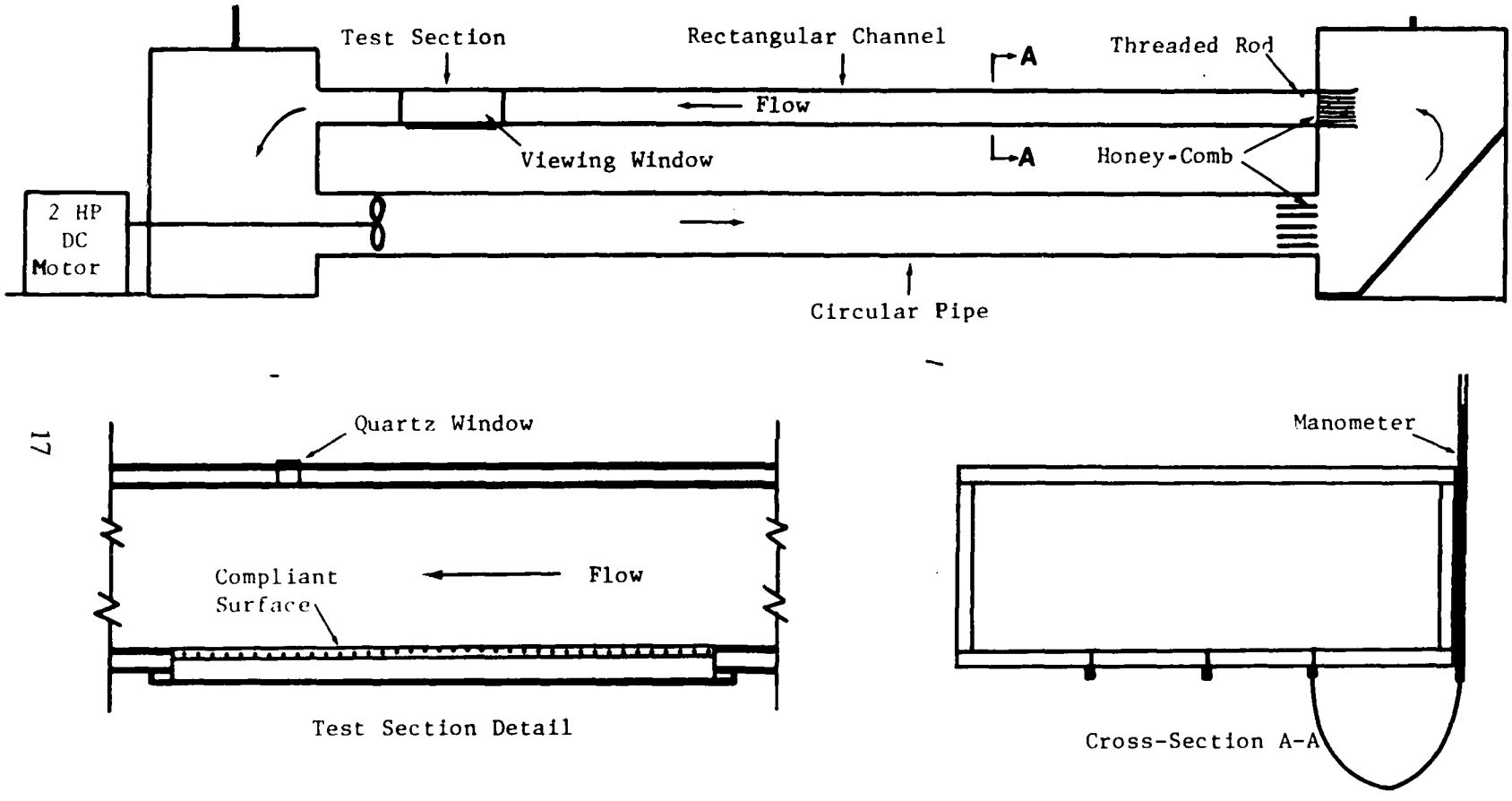

Fig. 1 A schematic of the kerosene channel flow facility.

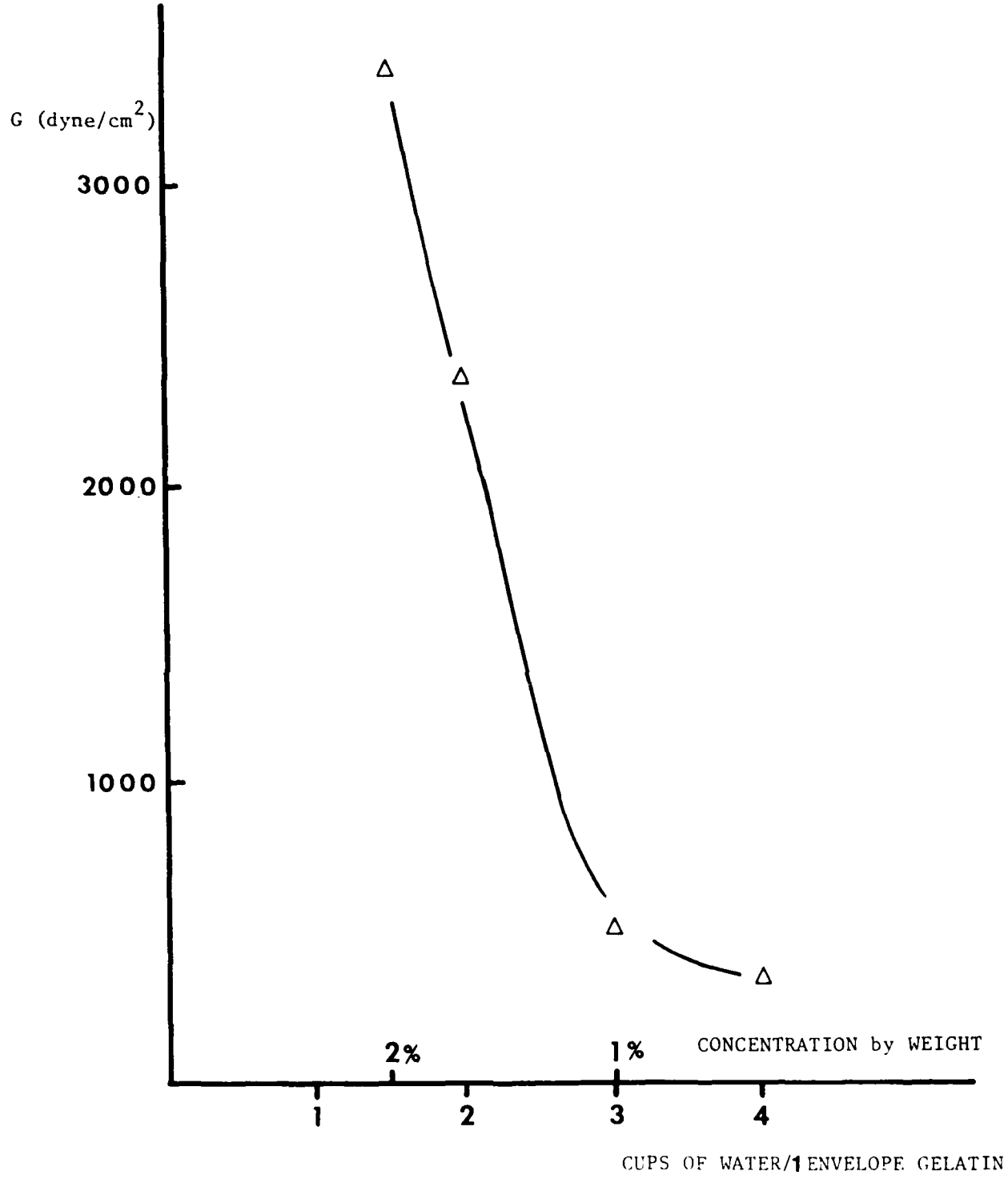

Fig. 2 The dependence of the shear modulus of gelatin on the concentration of gelatin and water mixture.

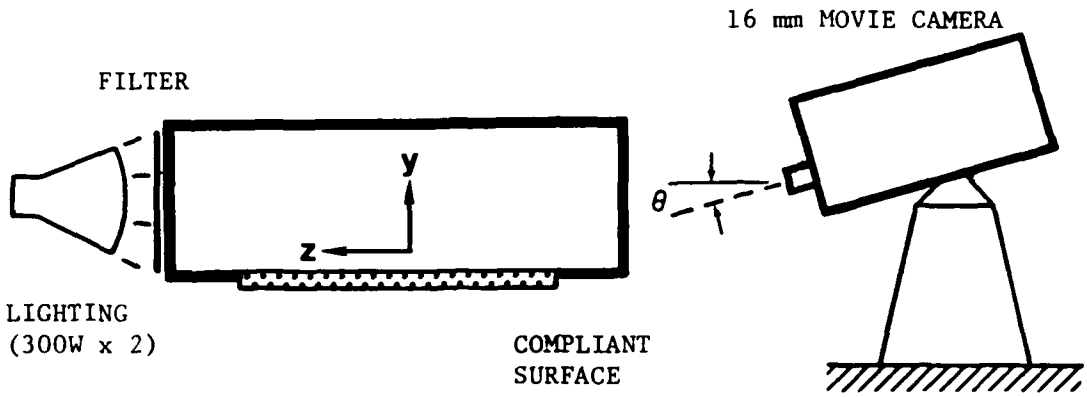

Fig. 3 A sketch of the experimental configuation used to capture the surface deformation under the turbulent channel flow.

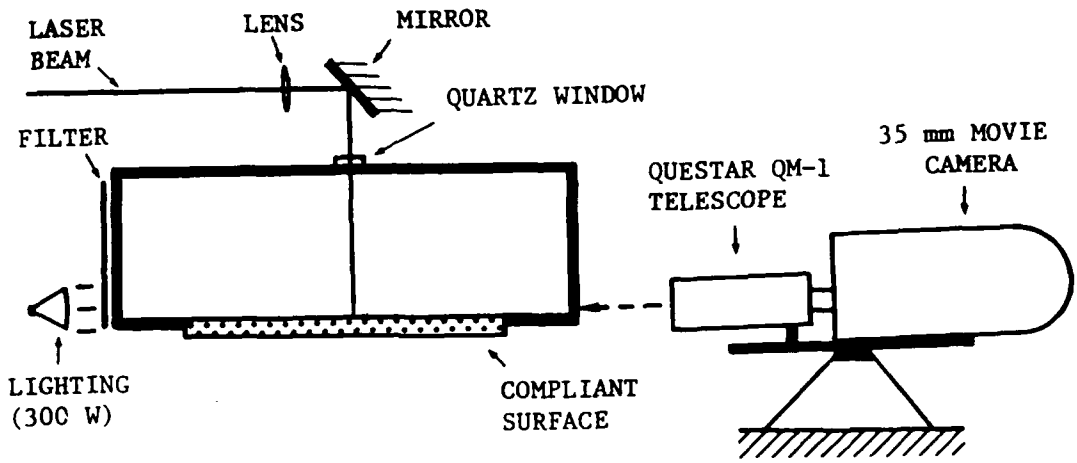

Fig. 4 The optical configuration of the wall shear stress measurement experiment.

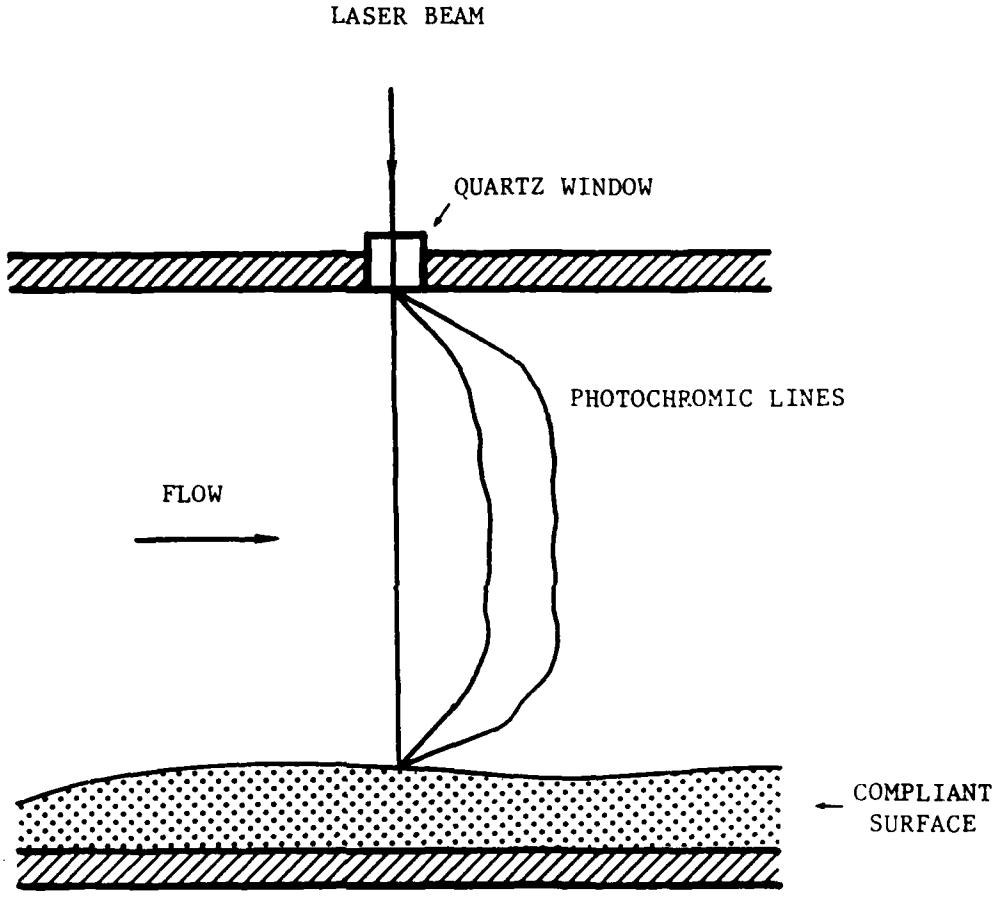

Fig. 5 A close-up of the technique used for the wall shear stress measurement on compliant surfaces.

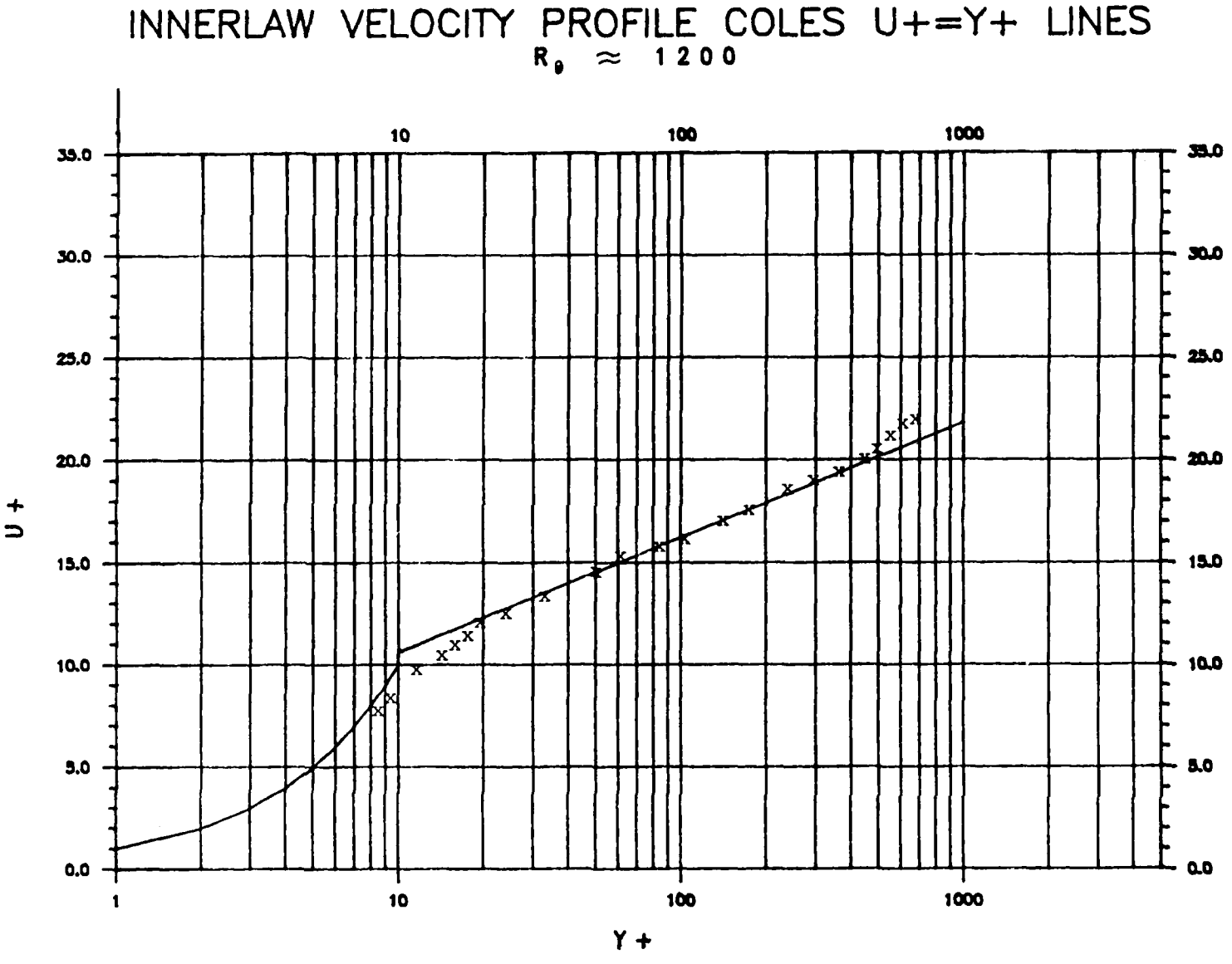

Fig. 6 The mean velocity profile over a stiff surface.(The centerline velocity is 0.341 m/sec yielding $R_\theta \approx 1200$).

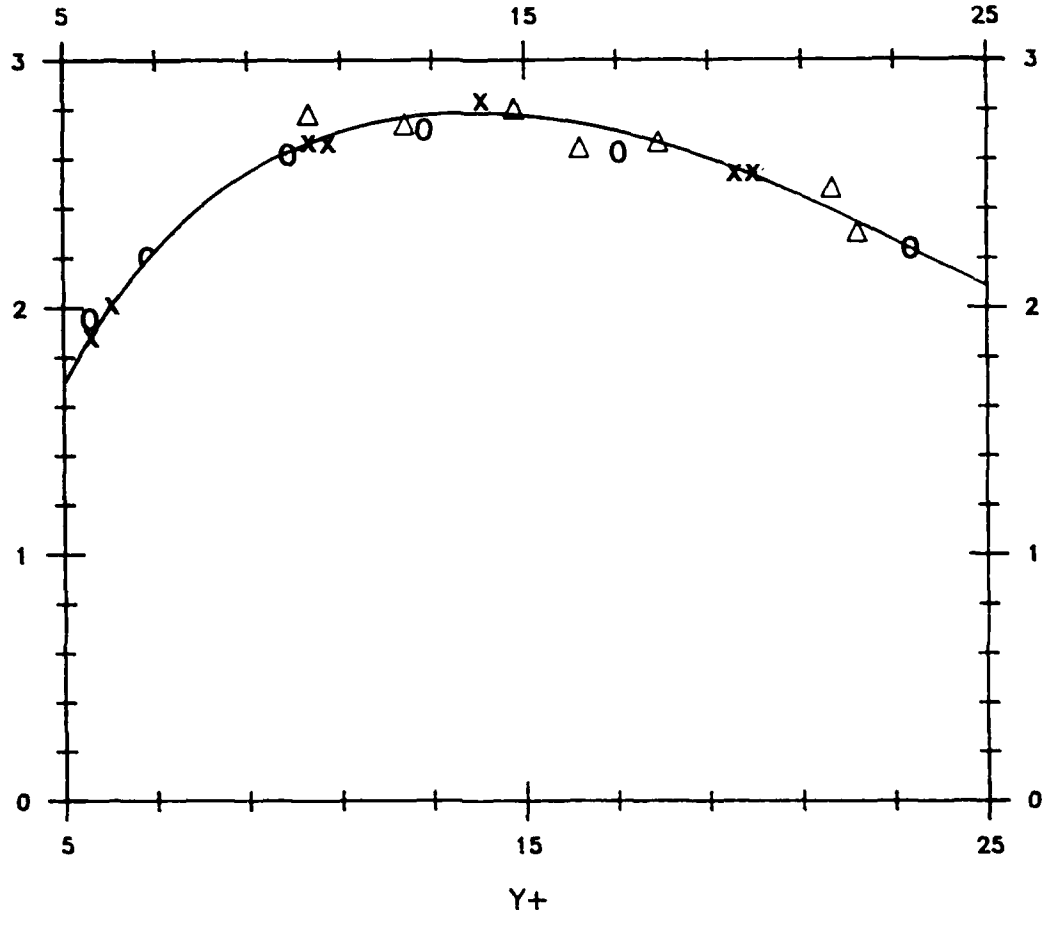

Fig. 7 The turbulent intensity profiles.

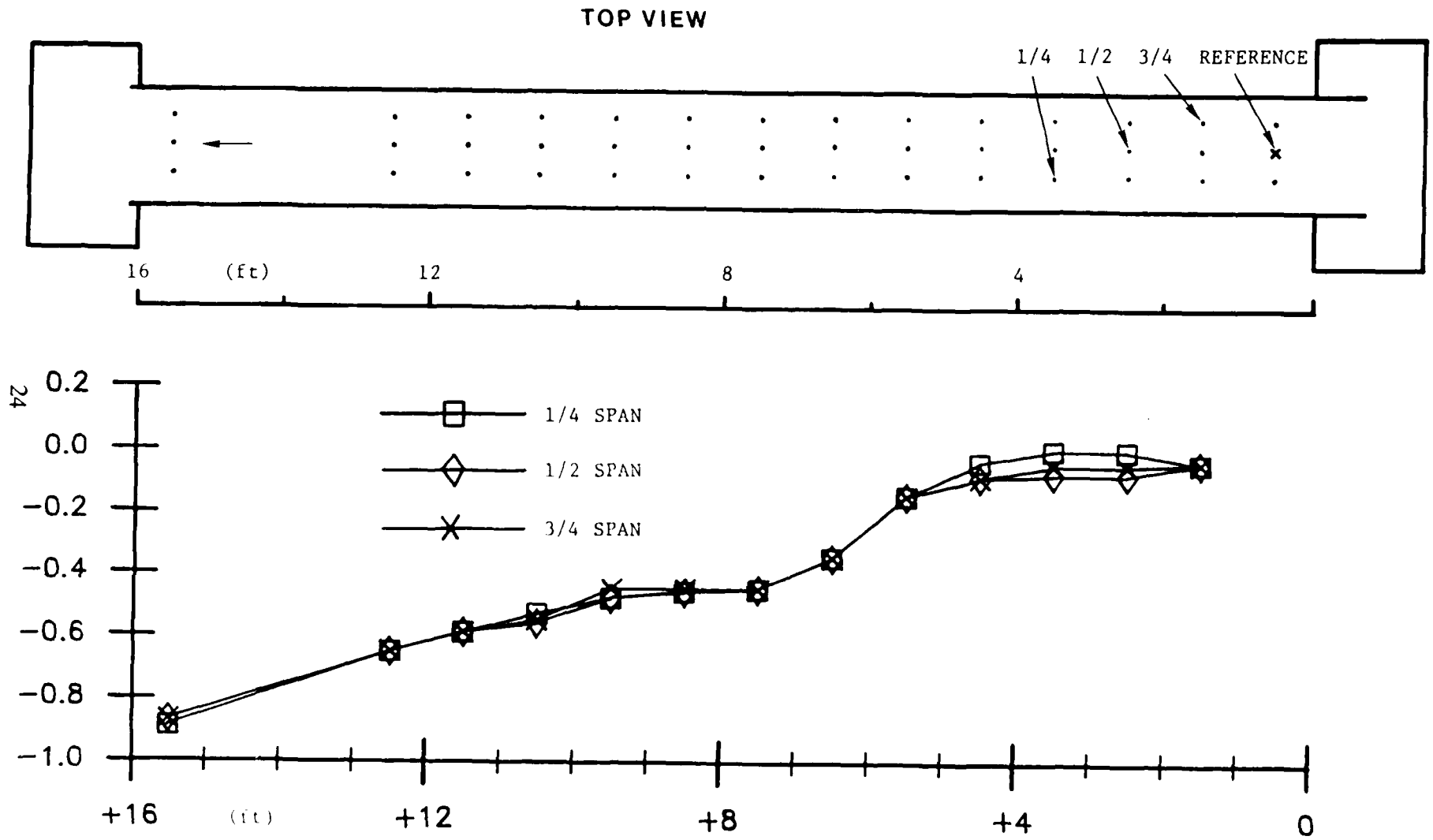

Fig. 8 The pressure distribution along the kerosene channel at $R_\theta \approx 1200$.

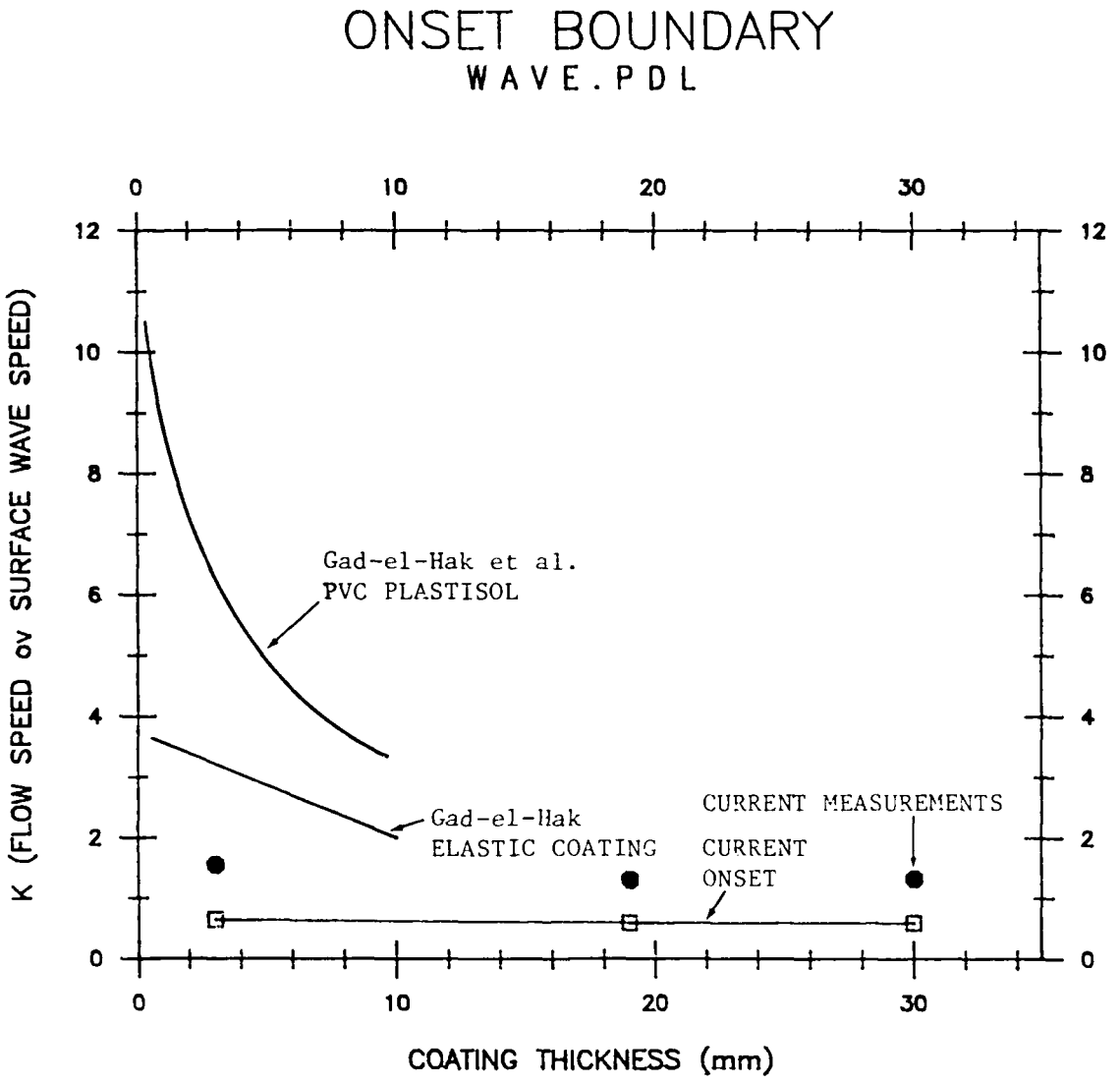

Fig. 9 The onset boundary for different compliant coatings.

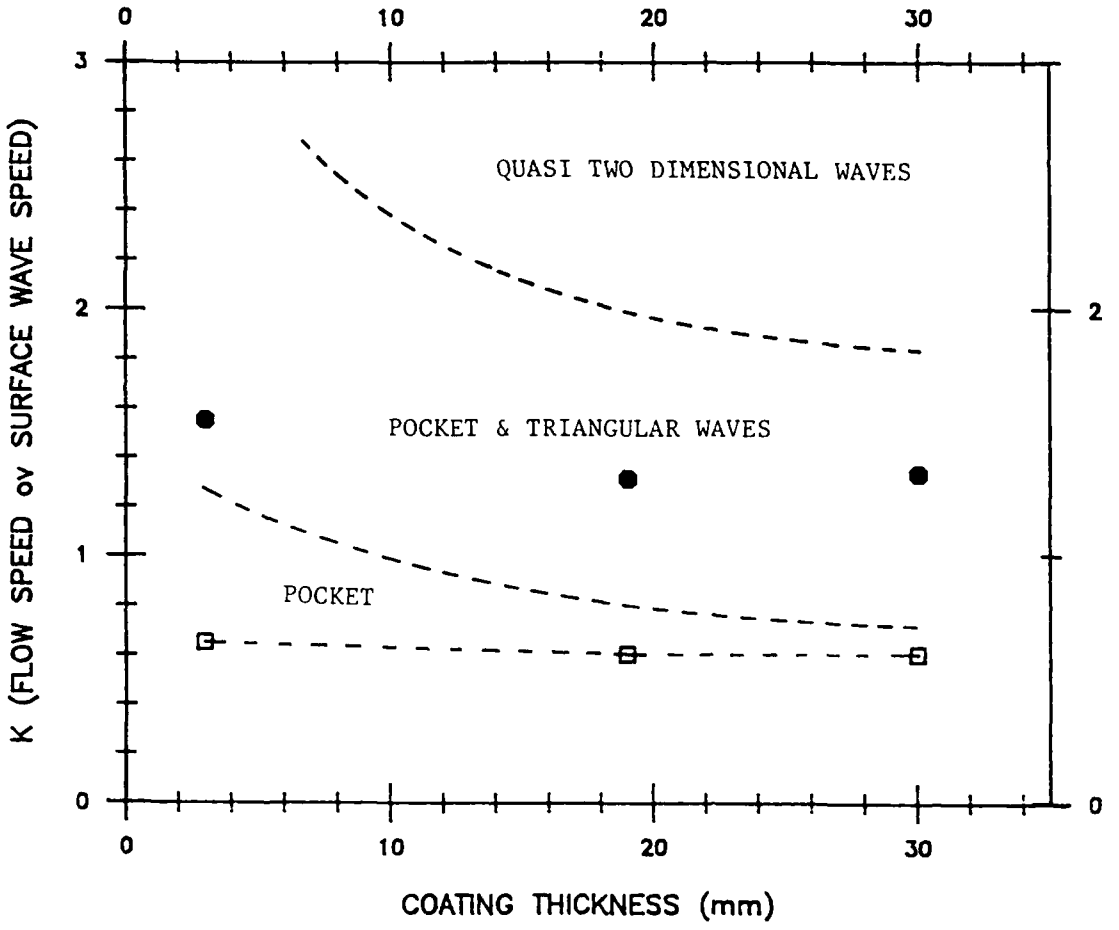

Fig. 10 The dependence of the occurrence of each element on both K and coating thickness.

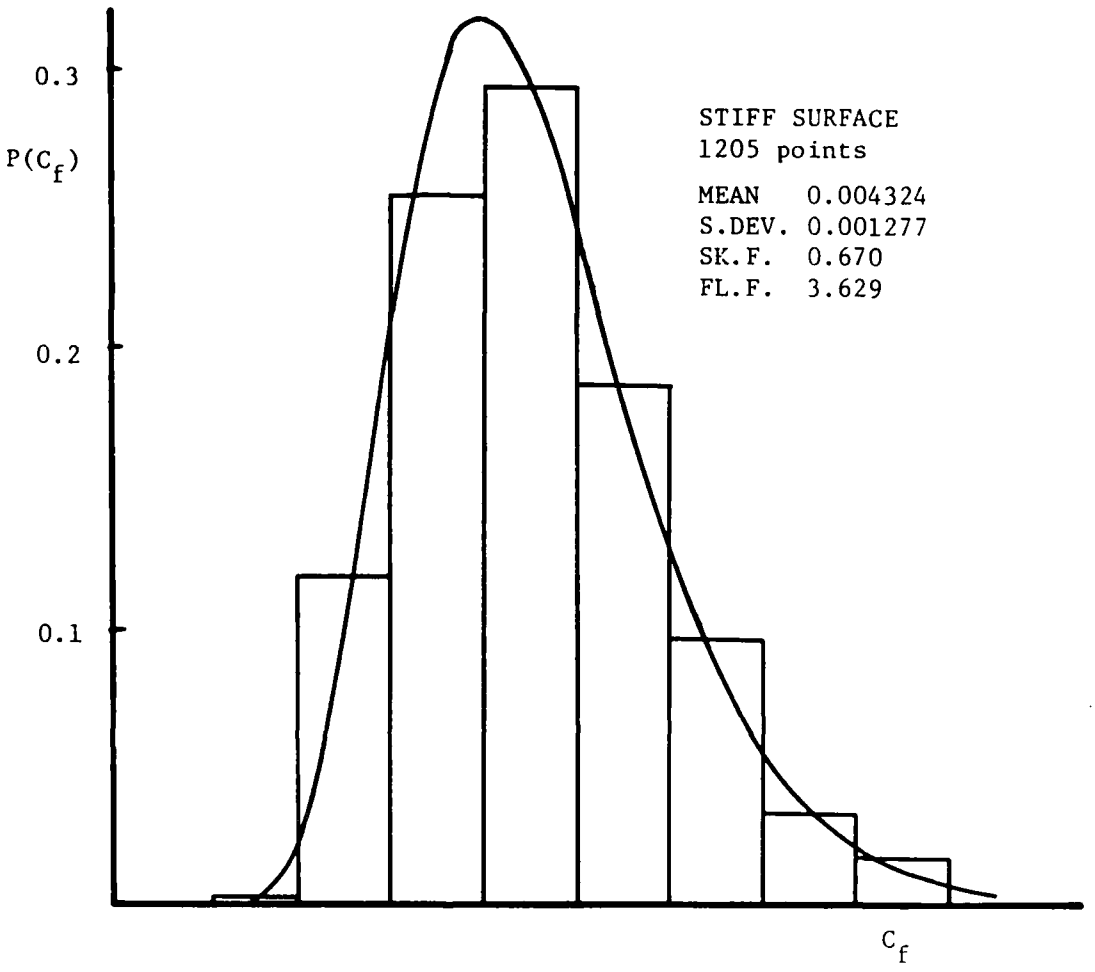

Fig. 11 The histogram of the skin friction obtained from 1205 samples over the reference stiff surface.

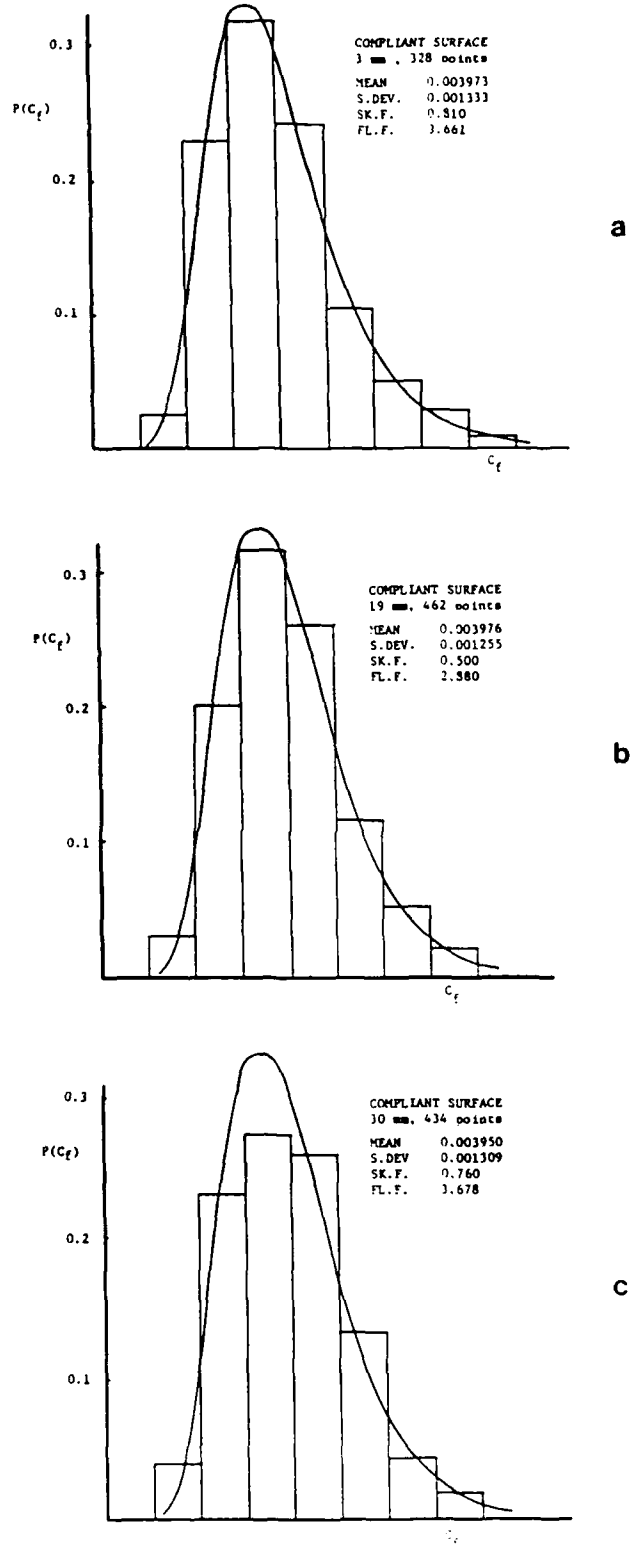

Fig. 12 The histograms of the skin friction associated with 3, 19 and 30 mm compliant coatings.

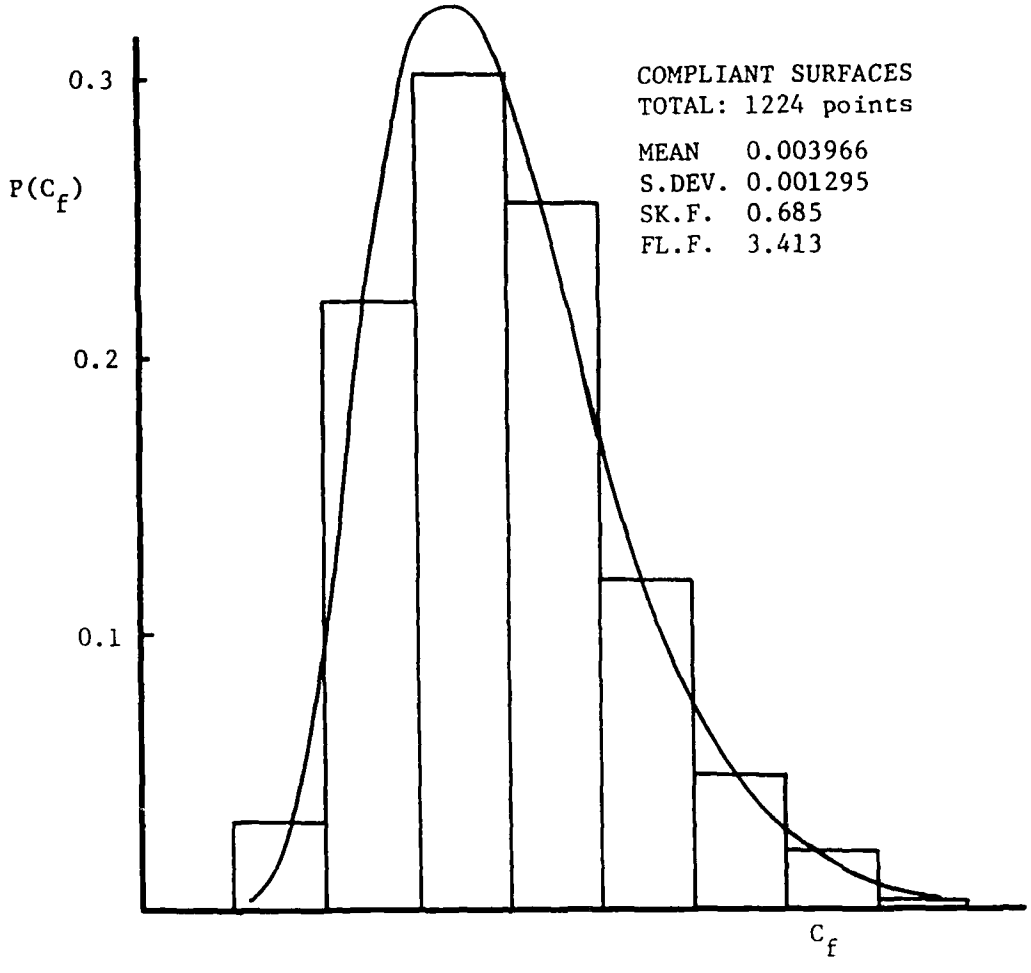

Fig. 13 The combination of Fig. 3.13 (a) through (c) regardless of thickness.

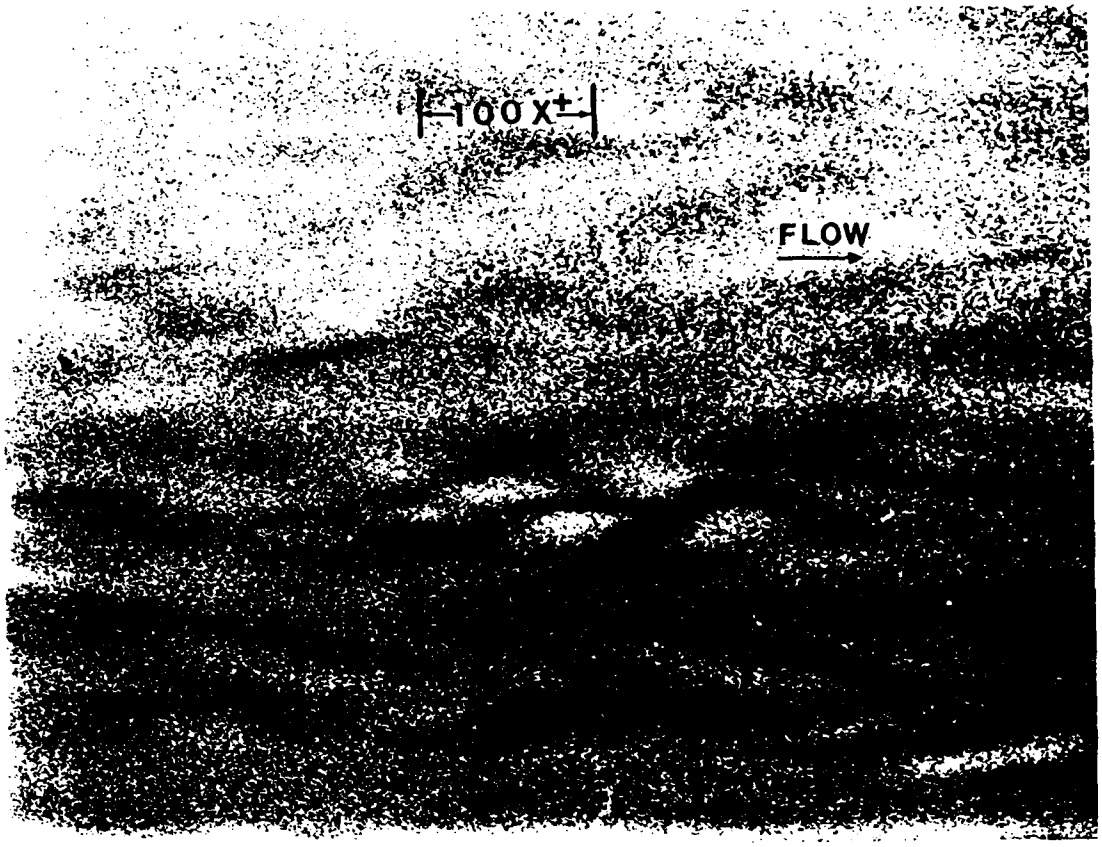

Fig. 14 A photo of the pocket-like depressions formed on the 3mm compliant surface.

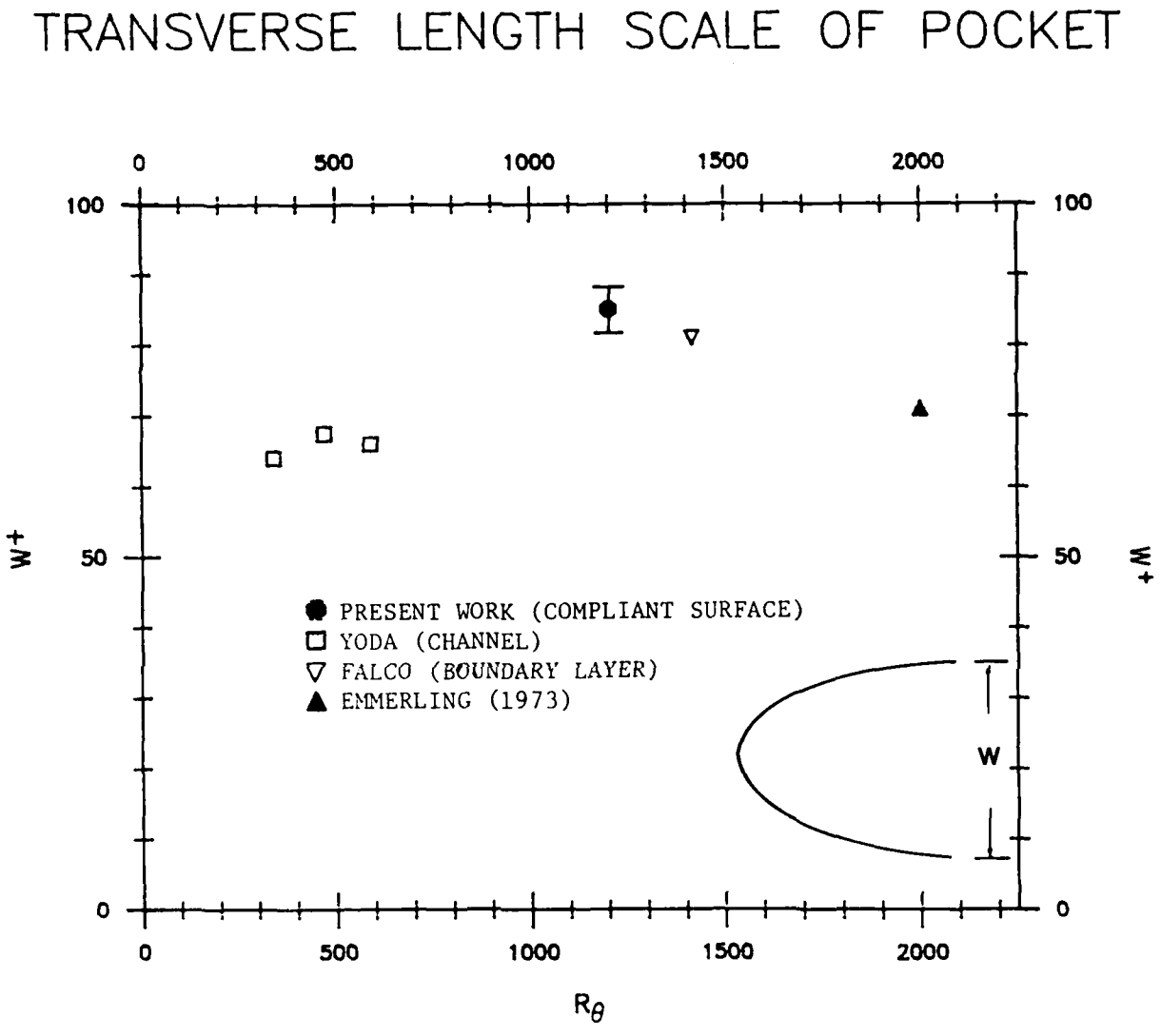

Fig. 15 The comparison of tranverse length scale of depressions in compliant surfaces with the pocket footprints made on a solid surface.

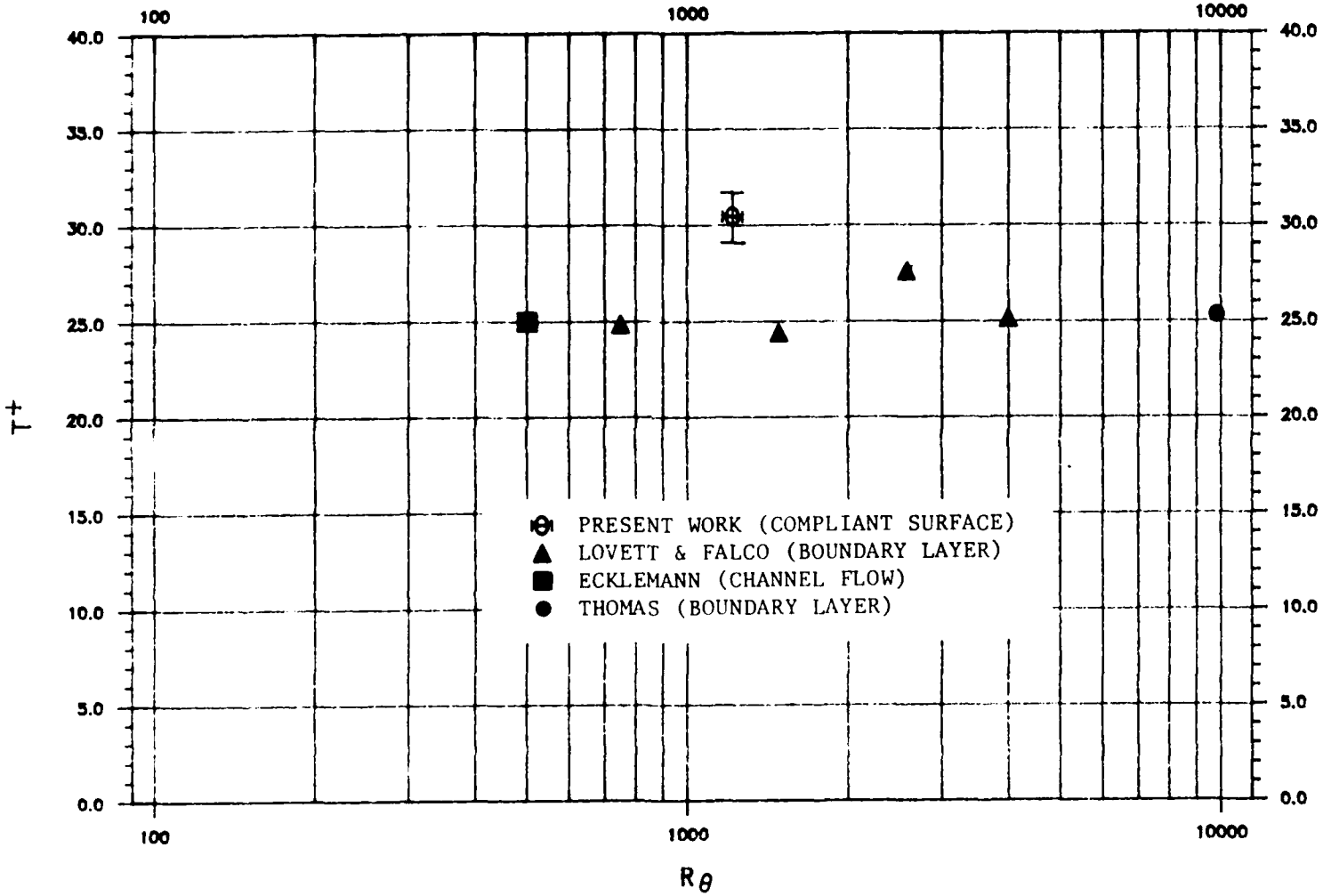

Fig. 16 The comparison of the time between pocket-like depressions in compliant surfaces with that obtained from boundary layer and channel flows.

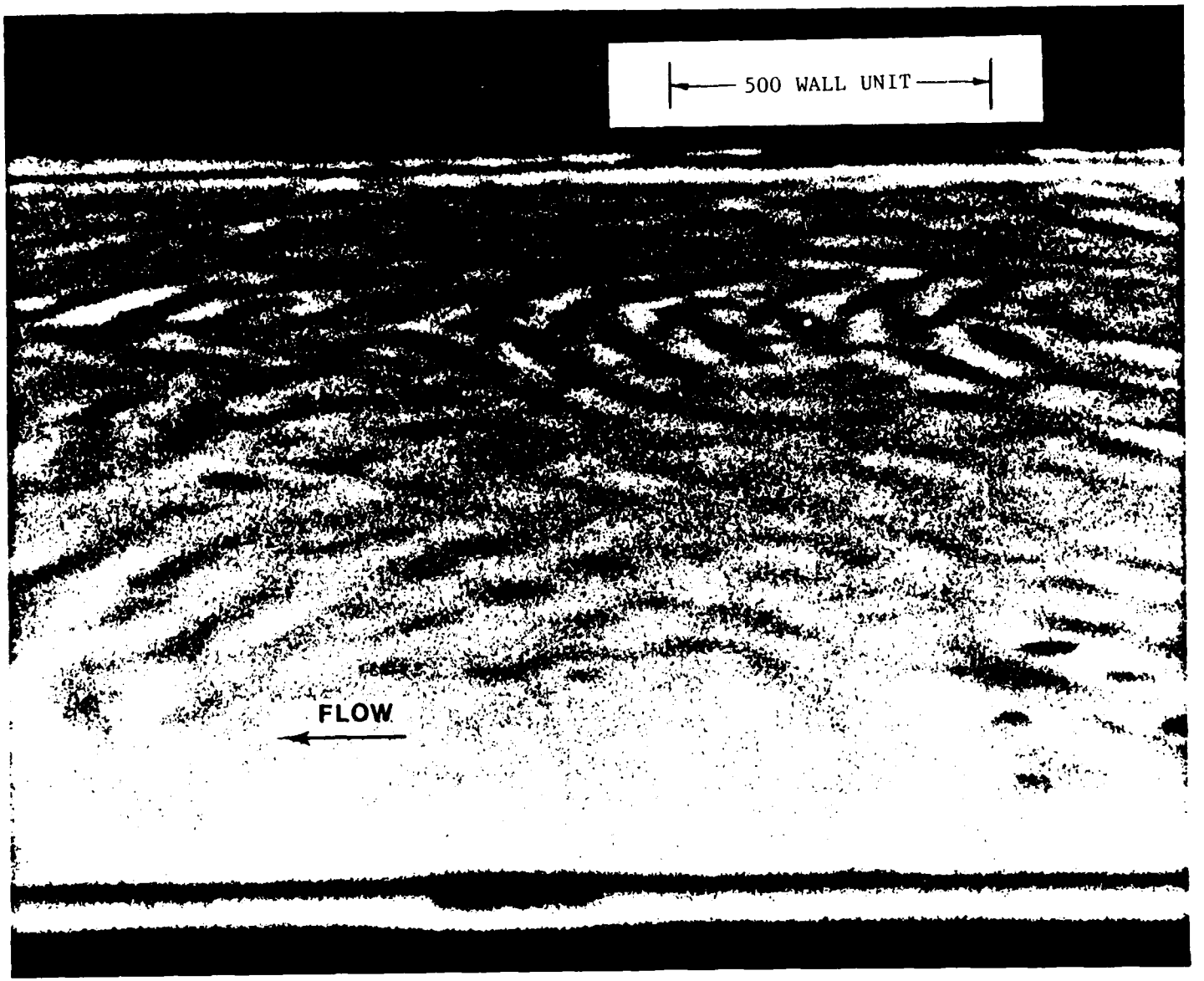

Fig. 17 A photo showing the triangle-like waves.

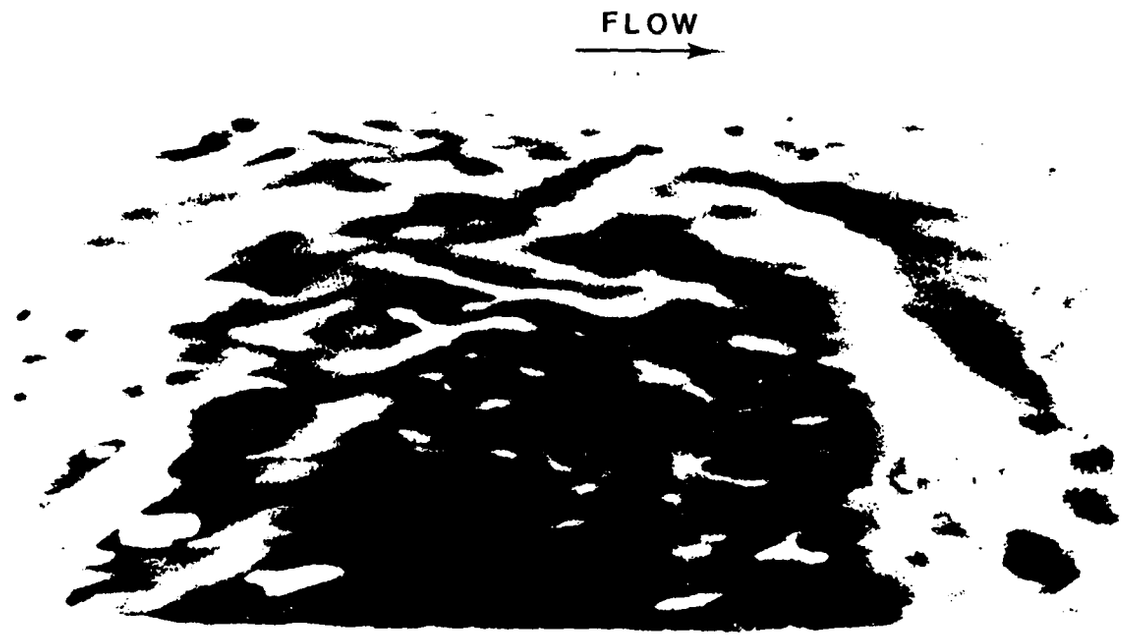

Fig. 18 A photo of the quasi two-dimensional large-scaled waves.

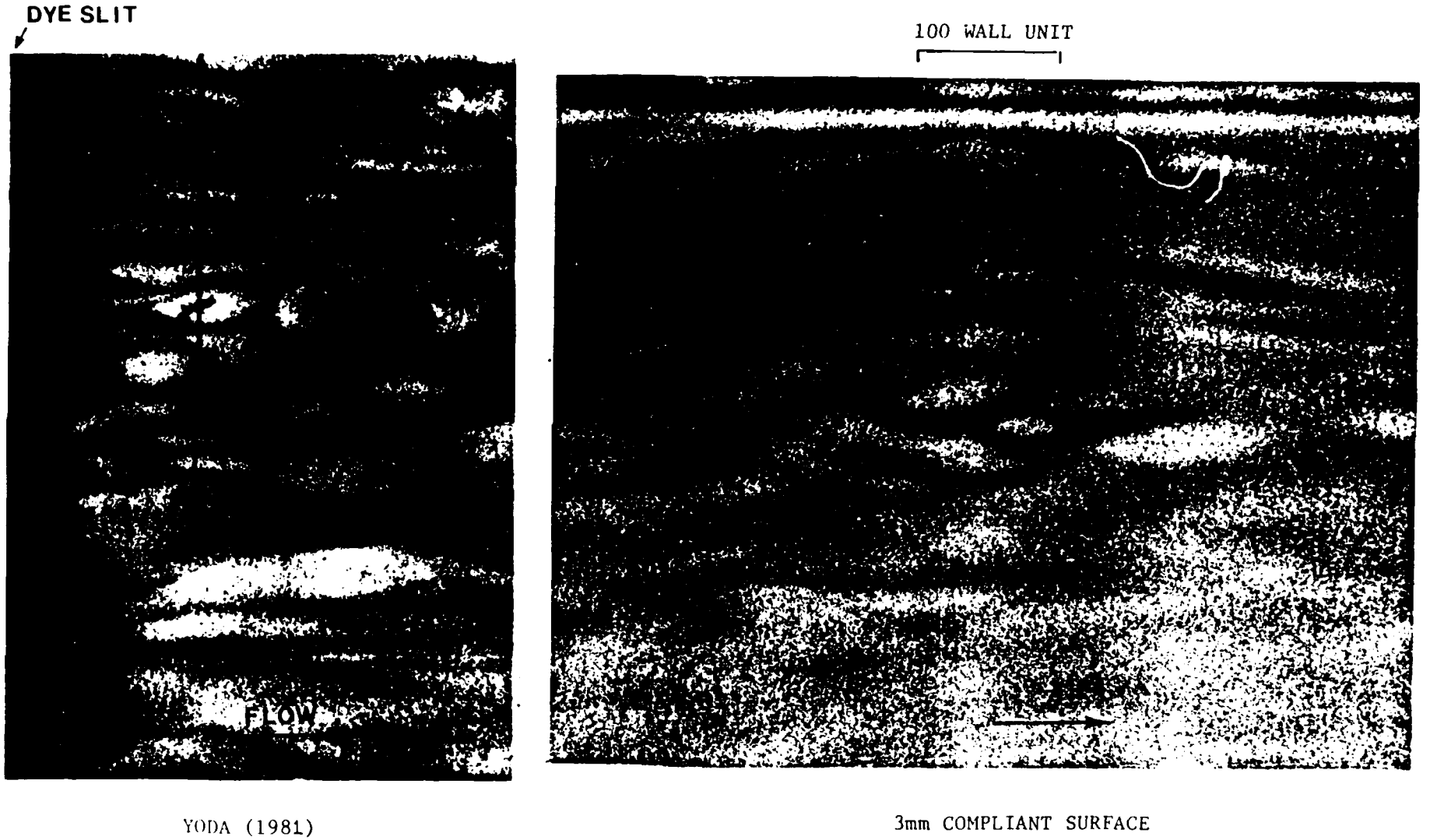

Fig. 19 A comparison of the visual phenomena on compliant surfaces with the flow visualization in the near wall region of channel flow by Yoda (1981).

END

DATE

FILMED

8-88

DTIC